Engineering Analysis with Boundary Elements 37 (2013) 673–682

Contents lists available at SciVerse ScienceDirect

Engineering Analysis with Boundary Elements

journal homepage: www.elsevier.com/locate/enganabound

The MLPG analyses of large deflections of magnetoelectroelastic plates

J. Sladek [a,*], V. Sladek [a], S. Krahulec [a], E. Pan [b]

[a] Institute of Construction and Architecture, Slovak Academy of Sciences, 84503 Bratislava, Slovakia
[b] Department of Civil Engineering, University of Akron, Akron, OH 44325-3905, USA

ARTICLE INFO

Article history:
Received 20 November 2012
Accepted 5 February 2013

Keywords:
Local integral equations
von Karman plate theory
Time-harmonic load
MLS approximation
Sensor
Actuator

ABSTRACT

The von Karman plate theory of large deformations is applied to express the strains, which are then used in the constitutive equations for magnetoelectroelastic solids. The in-plane electric and magnetic fields can be ignored for plates. A quadratic variation of electric and magnetic potentials along the thickness direction of the plate is assumed. The number of unknown terms in the quadratic approximation is reduced, satisfying the Maxwell equations. Bending moments and shear forces are considered by the Reissner–Mindlin theory, and the original three-dimensional (3D) thick plate problem is reduced to a two-dimensional (2D) one. A meshless local Petrov–Galerkin (MLPG) method is applied to solve the governing equations derived based on the Reissner–Mindlin theory. Nodal points are randomly distributed over the mean surface of the considered plate. Each node is the centre of a circle surrounding it. The weak form on small subdomains with a Heaviside step function as the test function is applied to derive the local integral equations. After performing the spatial MLS approximation, a system of algebraic equations for certain nodal unknowns is obtained. Both stationary and time-harmonic loads are then analyzed numerically.

1. Introduction

Magnetoelectroelastic (MEE) materials have found much application as sensors and actuators for the purpose of monitoring and controlling the response of structures. The MEE layers are frequently embedded into laminated composite plates to control the shape of plates. The magneto-electric forces give raise to strains that could reduce the effects of the applied mechanical load. Hence, advanced structures can be designed using less material and hence less weight. Pan [1] and Pan and Heyliger [2] presented analytical solutions for the analysis of simply supported MEE laminated rectangular plates, under static deformation and free vibration. Recently, Wu et al. [3] extended the Pagano solution for the three-dimensional (3D) plate problem to the analysis of a simply supported, functionally graded rectangular plate under MEE loads. Liu and Chang [4] studied the vibration of a MEE rectangular plate. To the authors' knowledge, little work has been carried out on the geometrically nonlinear problems occurred at large plate deformations. So far, only one paper [5] is dealing with the nonlinear behaviour of a MEE plate, where a simplified analytical solution was given for a thin simply supported MEE plate under a large deformation. The Kirchhoff plate bending theory with vanishing shear stresses was utilized.

The conventional von Karman-type nonlinear field equations for the finite deflection of plates are based on the Kirchhoff-Love assumption and follow inevitable coupling between in-plane and bending deformations, which makes analytical solutions difficult. Therefore, a simplified governing field equation known as the decoupled Berger equation [6] is also used for geometrically nonlinear deformation of plates. The Berger equation could be a fairly good approximation to the corresponding rigorous solution, provided that the in-plane displacements are constrained at the boundary [7]. Among the early proposals for analysing the final deflection of thin plates is the work by Kamiya and Sawaki [8]. The first finite element analysis of geometrically nonlinear plate behaviour using a Mindlin formulation was given by Pica et al. [9]. The boundary element method (BEM) was applied by Lei et al. [10] in the geometrically nonlinear analysis of laterally loaded isotropic plates, taking into account the effect of transverse shear deformation. A nonlinear analysis of Reissner plates by BEM was given by Qin [11]. Wen et al. [12] analyzed the post-buckling of Reissner plates. Recently, a strong formulation with multiquadric radial basis function was applied to the isotropic Reissner–Mindlin plates with geometrical nonlinearity [13].

The solution of the boundary or initial boundary value problems for MEE plates with large deformations requires advanced numerical methods due to the high mathematical complexity. Besides the well established finite element method (FEM) and the BEM [14,15], the meshless methods provide an efficient and popular alternative to these traditional computational methods.

* Corresponding author. Tel./fax: +421 2 54773548.
E-mail address: jan.sladek@savba.sk (J. Sladek).

0955-7997/$ - see front matter © 2013 Elsevier Ltd. All rights reserved.
http://dx.doi.org/10.1016/j.enganabound.2013.02.001

Focusing only on nodes or points instead of elements used in the conventional FEM, meshless approaches have certain advantages. The elimination of shear locking in thin walled structures by FEM is difficult and the developed techniques are less accurate. The moving least-square (MLS) approximation ensures C^1 continuity which satisfies the Kirchhoff hypotheses. The continuity of the MLS approximation is given by the minimum between the continuity of the basis functions and that of the weight function. So continuity can be tuned to a desired degree. Previous results showed excellent convergence for linear problems [16–18], however, up to now the formulation has not been applied to large deflection of MEE plate problems. Recently, new class of hybrid/mixed finite elements, denoted as HMFEM-C, was developed for modelling two-dimensional (2D) problems in MEE materials [19]. These elements were based on assuming first the independent strain, electric and magnetic fields, and then collocating them with the strain, electric and magnetic fields derived from the primal variables (mechanical displacement, electric and magnetic potentials) at certain selected points inside each element. The newly developed elements showed significantly higher accuracy than the primal elements for the electric, magnetic as well as the mechanical variables, comparable to the accuracy from the meshless approach [19]. Up to date, however, these hybrid finite elements have not been applied to plate bending problems.

One of the most rapidly developed meshfree methods is the meshless local Petrov–Galerkin (MLPG) method [20]. The MLPG method has attracted much attention in the past decade and it has been successfully applied also to plate problems [21–24]. The modelling of piezoelectric plates has been done by the MLPG too [25,26].

This paper proposes a nonlinear (or large-deformation) model for the MEE thick plate under a static and time-harmonic mechanical load and a stationary electromagnetic load. It is the first effort to develop the meshless method based on the local Petrov–Galerkin weak-form to solve dynamic problems for thick MEE plates under a large deformation described by the Reissner–Mindlin theory. The electric and magnetic field components are assumed to be zero in the in-plane directions of the plate. A quadratic power-expansion of the electric and magnetic potentials in the thickness direction of the plate is considered. The bending moment, normal and shear force expressions are obtained by integration through the plate for the considered constitutive equations. The Reissner–Mindlin governing equations of motion are subsequently solved for a time-harmonic plate bending problem. The Reissner–Mindlin theory reduces the original 3D thick plate problem to a 2D problem. In our meshless method, nodal points are randomly distributed over the neutral plane of the considered plate. Each node is the centre of a circle surrounding this node. The weak form on the small subdomains with a Heaviside step function as the test function is applied to derive local integral equations. Applying the Gauss divergence theorem to the weak form, the local boundary-domain integral equations are derived. The nonlinear terms occurred in the normal and shear forces are considered iteratively in the full-load algorithm. After performing the spatial MLS approximation, a system of algebraic equations for certain nodal unknowns is obtained. Numerical examples are presented and discussed to show the accuracy and the efficiency of the present method.

2. Local integral equations for magnetoelectroelastic plates

We consider a plate of total thickness h with homogeneous MEE material properties with its mean surface occupying the domain Ω in the plane (x_1,x_2). The axis $x_3 \equiv z$ is perpendicular to the mid-plane (Fig. 1) with the origin at the bottom of the plate.

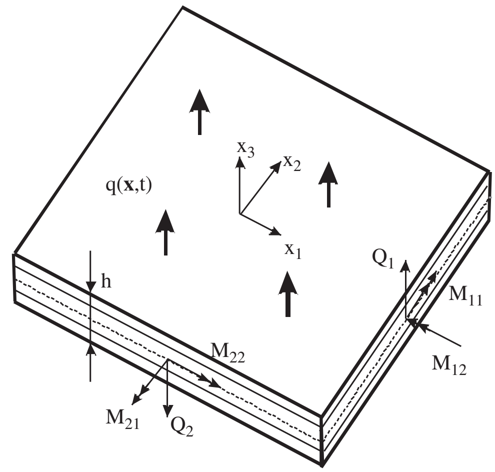

Fig. 1. Sign convention of bending moments and forces for a plate.

The Cartesian coordinate system is introduced such that the bottom and top surfaces of plate is placed in the plane $z=0$ and $z=$h, respectively. Using the von Karman theory of large deflection of plates described by the Reissner–Mindlin theory, the Lagrangian strain displacement relations are given by Pica et al. [9] and Azizian and Dawe [27]:

$$
\begin{aligned}
&\varepsilon_{11}(\mathbf{x},x_3,\tau) = u_{0,1} + (z-z_0)w_{1,1}(\mathbf{x},\tau) + \frac{1}{2}(w_{3,1}(\mathbf{x},\tau))^2,\\
&\varepsilon_{22}(\mathbf{x},x_3,\tau) = v_{0,2} + (z-z_0)w_{2,2}(\mathbf{x},\tau) + \frac{1}{2}(w_{3,2}(\mathbf{x},\tau))^2,\\
&\varepsilon_{12}(\mathbf{x},x_3,\tau) = \frac{1}{2}(u_{0,2}+v_{0,1}) + \frac{1}{2}(z-z_0)\left[w_{1,2}(\mathbf{x},\tau)+w_{2,1}(\mathbf{x},\tau)\right]\\
&\qquad\qquad + \frac{1}{2}w_{3,1}(\mathbf{x},\tau)w_{3,2}(\mathbf{x},\tau),\\
&\varepsilon_{13}(\mathbf{x},\tau) = [w_1(\mathbf{x},\tau)+w_{3,1}(\mathbf{x},\tau)]/2,\\
&\varepsilon_{23}(\mathbf{x},\tau) = [w_2(\mathbf{x},\tau)+w_{3,2}(\mathbf{x},\tau)]/2. \qquad (1)
\end{aligned}
$$

where z_0 indicates the position of the neutral plane. For a homogeneous plate it is located in the geometrical mid-plane. In-plane displacements in x_1- and x_2-directions are denoted by u_0 and v_0. Rotations around x_2- and x_1-axes are denoted by w_1 and w_2, and w_3 is the out-of-plane deflection.

The constitutive equations for the stress tensor, electrical displacement and magnetic induction of the MEE materials are given by Nan [28]:

$$\sigma_{ij}(\mathbf{x},x_3,\tau) = c_{ijkl}\varepsilon_{kl}(\mathbf{x},x_3,\tau) - e_{kij}E_k(\mathbf{x},x_3,\tau) - d_{kij}H_k(\mathbf{x},x_3,\tau), \qquad (2)$$

$$D_j(\mathbf{x},x_3,\tau) = e_{jkl}\varepsilon_{kl}(\mathbf{x},x_3,\tau) + h_{jk}E_k(\mathbf{x},x_3,\tau) + \alpha_{jk}H_k(\mathbf{x},x_3,\tau), \qquad (3)$$

$$B_j(\mathbf{x},x_3,\tau) = d_{jkl}\varepsilon_{kl}(\mathbf{x},x_3,\tau) + \alpha_{kj}E_k(\mathbf{x},x_3,\tau) + \gamma_{jk}H_k(\mathbf{x},x_3,\tau), \qquad (4)$$

where $\{\varepsilon_{ij},E_i,H_i\}$ is the set of the secondary field quantities (strain, intensity of electric field, intensity of magnetic field) which are expressed in terms of the gradients of the primary fields, i.e., the elastic displacement vector, electric potential, and magnetic potential $\{u_i,\phi,\psi\}$. Finally, the elastic stress tensor, electric displacement, and magnetic induction vectors $\{\sigma_{ij},D_i,B_i\}$ form the set of the fields conjugated to the secondary fields $\{\varepsilon_{ij},E_i,H_i\}$. The constitutive equations correlate these two sets of fields in continuum media including the multi-field interactions.

The plate thickness is assumed to be small as compared to its in-plane dimensions. The normal stress σ_{33} is then vanishing in comparison with other normal stresses. Assuming also that the MEE materials process certain material symmetry, one can formulate the plane-deformation problems [29]. For instance, for the poling direction along the positive x_3-axis the constitutive

Eqs. (2)–(4) are reduced to the following matrix forms:

$$\begin{bmatrix}\sigma_{11}\\ \sigma_{22}\\ \sigma_{12}\\ \sigma_{13}\\ \sigma_{23}\end{bmatrix}=\begin{bmatrix}c_{11} & c_{12} & 0 & 0 & 0\\ c_{12} & c_{22} & 0 & 0 & 0\\ 0 & 0 & c_{66} & 0 & 0\\ 0 & 0 & 0 & c_{55} & 0\\ 0 & 0 & 0 & 0 & c_{44}\end{bmatrix}\begin{bmatrix}\varepsilon_{11}\\ \varepsilon_{22}\\ 2\varepsilon_{12}\\ 2\varepsilon_{13}\\ 2\varepsilon_{23}\end{bmatrix}-\begin{bmatrix}0 & 0 & e_{31}\\ 0 & 0 & e_{32}\\ 0 & 0 & 0\\ e_{15} & 0 & 0\\ 0 & e_{15} & 0\end{bmatrix}$$

$$\times\begin{bmatrix}E_1\\ E_2\\ E_3\end{bmatrix}-\begin{bmatrix}0 & 0 & d_{31}\\ 0 & 0 & d_{32}\\ 0 & 0 & 0\\ d_{15} & 0 & 0\\ 0 & d_{15} & 0\end{bmatrix}\begin{bmatrix}H_1\\ H_2\\ H_3\end{bmatrix}$$

$$\equiv \mathbf{C}\begin{bmatrix}\varepsilon_{11}\\ \varepsilon_{22}\\ 2\varepsilon_{12}\\ 2\varepsilon_{13}\\ 2\varepsilon_{23}\end{bmatrix}-\mathbf{L}\begin{bmatrix}E_1\\ E_2\\ E_3\end{bmatrix}-\mathbf{K}\begin{bmatrix}H_1\\ H_2\\ H_3\end{bmatrix}, \tag{5}$$

$$\begin{bmatrix}D_1\\ D_2\\ D_3\end{bmatrix}=\begin{bmatrix}0 & 0 & 0 & e_{15} & 0\\ 0 & 0 & 0 & 0 & e_{15}\\ e_{31} & e_{32} & 0 & 0 & 0\end{bmatrix}\begin{bmatrix}\varepsilon_{11}\\ \varepsilon_{22}\\ 2\varepsilon_{12}\\ 2\varepsilon_{13}\\ 2\varepsilon_{23}\end{bmatrix}+\begin{bmatrix}h_{11} & 0 & 0\\ 0 & h_{22} & 0\\ 0 & 0 & h_{33}\end{bmatrix}$$

$$\times\begin{bmatrix}E_1\\ E_2\\ E_3\end{bmatrix}+\begin{bmatrix}\alpha_{11} & 0 & 0\\ 0 & \alpha_{22} & 0\\ 0 & 0 & \alpha_{33}\end{bmatrix}\begin{bmatrix}H_1\\ H_2\\ H_3\end{bmatrix}$$

$$\equiv \mathbf{G}\begin{bmatrix}\varepsilon_{11}\\ \varepsilon_{22}\\ 2\varepsilon_{12}\\ 2\varepsilon_{13}\\ 2\varepsilon_{23}\end{bmatrix}+\mathbf{H}\begin{bmatrix}E_1\\ E_2\\ E_3\end{bmatrix}+\mathbf{A}\begin{bmatrix}H_1\\ H_2\\ H_3\end{bmatrix}, \tag{6}$$

$$\begin{bmatrix}B_1\\ B_2\\ B_3\end{bmatrix}=\begin{bmatrix}0 & 0 & 0 & d_{15} & 0\\ 0 & 0 & 0 & 0 & d_{15}\\ d_{31} & d_{32} & 0 & 0 & 0\end{bmatrix}\begin{bmatrix}\varepsilon_{11}\\ \varepsilon_{22}\\ 2\varepsilon_{12}\\ 2\varepsilon_{13}\\ 2\varepsilon_{23}\end{bmatrix}+\begin{bmatrix}\alpha_{11} & 0 & 0\\ 0 & \alpha_{22} & 0\\ 0 & 0 & \alpha_{33}\end{bmatrix}$$

$$\times\begin{bmatrix}E_1\\ E_2\\ E_3\end{bmatrix}+\begin{bmatrix}\gamma_{11} & 0 & 0\\ 0 & \gamma_{22} & 0\\ 0 & 0 & \gamma_{33}\end{bmatrix}\begin{bmatrix}H_1\\ H_2\\ H_3\end{bmatrix}$$

$$\equiv \mathbf{R}\begin{bmatrix}\varepsilon_{11}\\ \varepsilon_{22}\\ 2\varepsilon_{12}\\ 2\varepsilon_{13}\\ 2\varepsilon_{23}\end{bmatrix}+\mathbf{A}\begin{bmatrix}E_1\\ E_2\\ E_3\end{bmatrix}+\mathbf{M}\begin{bmatrix}H_1\\ H_2\\ H_3\end{bmatrix}. \tag{7}$$

The vector Maxwell's equations in quasi-static approximation are satisfied if the electric and magnetic fields are expressed as gradients of the scalar electric and magnetic potentials $\phi(\mathbf{x},\tau)$ and $\psi(\mathbf{x},\tau)$, respectively [29]:

$$E_j=-\phi_{,j}, \tag{8}$$

$$H_j=-\psi_{,j}. \tag{9}$$

Since the plate is relatively thin, the in-plane electric and magnetic fields can be ignored, i.e., $E_1=E_2=0$ and $H_1=H_2=0$ according Liu and Chang [4]. It is reasonable to further assume that $(|D_{1,1}|,|D_{2,2}|)\ll|D_{3,3}|$ [30] and $(|B_{1,1}|,|B_{2,2}|)\ll|B_{3,3}|$. Then, the Maxwell equations are reduced to

$$D_{3,3}=0, \tag{10}$$

$$B_{3,3}=0. \tag{11}$$

The electric and magnetic potentials in the plate are assumed to be varying quadratically in z direction:

$$\phi(\mathbf{x},z,\tau)=\phi_0(\mathbf{x},\tau)+\phi_1(\mathbf{x},\tau)\frac{z-z_0}{h}+\phi_2(\mathbf{x},\tau)\left(\frac{z-z_0}{h}\right)^2, \tag{12}$$

$$\psi(\mathbf{x},z,\tau)=\psi_0(\mathbf{x},\tau)+\psi_1(\mathbf{x},\tau)\frac{z-z_0}{h}+\psi_2(\mathbf{x},\tau)\left(\frac{z-z_0}{h}\right)^2. \tag{13}$$

Substituting potentials (12) and (13) into the electrical displacement and magnetic induction expressions (6) and (7), one gets

$$\begin{aligned}D_3(\mathbf{x},z,\tau)&=e_{31}\left[u_{0,1}+w_{1,1}(\mathbf{x},\tau)(z-z_0)+\frac{1}{2}(w_{3,1})^2\right]\\&\quad+e_{32}\left[v_{0,2}+w_{2,2}(\mathbf{x},\tau)(z-z_0)+\frac{1}{2}(w_{3,2})^2\right]\\&\quad-h_{33}\frac{\phi_1(\mathbf{x},\tau)}{h}-2h_{33}\phi_2(\mathbf{x},\tau)\frac{z-z_0}{h^2}-\alpha_{33}\frac{\psi_1(\mathbf{x},\tau)}{h}\\&\quad-2\alpha_{33}\psi_2(\mathbf{x},\tau)\frac{z-z_0}{h^2},\end{aligned} \tag{14}$$

$$\begin{aligned}B_3(\mathbf{x},z,\tau)&=d_{31}\left[u_{0,1}+w_{1,1}(\mathbf{x},\tau)(z-z_0)+\frac{1}{2}(w_{3,1})^2\right]\\&\quad+d_{32}\left[v_{0,2}+w_{2,2}(\mathbf{x},\tau)(z-z_0)+\frac{1}{2}(w_{3,2})^2\right]\\&\quad-\alpha_{33}\frac{\phi_1(\mathbf{x},\tau)}{h}-2\alpha_{33}\phi_2(\mathbf{x},\tau)\frac{z-z_0}{h^2}-\gamma_{33}\frac{\psi_1(\mathbf{x},\tau)}{h}\\&\quad-2\gamma_{33}\psi_2(\mathbf{x},\tau)\frac{z-z_0}{h^2}.\end{aligned} \tag{15}$$

The remaining nonzero electric and magnetic field components are obtained by substituting the potentials (12) and (13) into Eqs. (8) and (9):

$$\begin{aligned}E_3(\mathbf{x},z,\tau)&=-\frac{\phi_1(\mathbf{x},\tau)}{h}-2\phi_2(\mathbf{x},\tau)\frac{z-z_0}{h^2},\\H_3(\mathbf{x},z,\tau)&=-\frac{\psi_1(\mathbf{x},\tau)}{h}-2\psi_2(\mathbf{x},\tau)\frac{z-z_0}{h^2}.\end{aligned} \tag{16}$$

One can define the integral quantities such as the bending moments $M_{\alpha\beta}$, normal forces $T_{\alpha\beta}$ and the shear forces Q_α [10] as

$$\begin{aligned}M_{\alpha\beta}&=\int_0^h\sigma_{\alpha\beta}(z-z_0)dz,\\T_{\alpha\beta}&=\int_0^h\sigma_{\alpha\beta}\,dz,\\Q_\alpha&=\kappa\int_0^h\sigma_{\alpha3}dz+\int_0^h\sigma_{\alpha\beta}w_{3,\beta}\,dz,\end{aligned} \tag{17}$$

where the Greek indices take values 1,2 and $\kappa=5/6$ according to the Reissner plate theory.

Substituting Eqs. (5) and (16) into the moment and force resultants (17) allows the expression of the bending moments $M_{\alpha\beta}$ and shear forces Q_α in terms of the rotations, deflection, electric and magnetic potential coefficients:

$$\begin{aligned}M_{11}(\mathbf{x},\tau)&=\int_0^h\left\{c_{11}\left[u_{0,1}+(z-z_0)w_{1,1}+\frac{1}{2}w_{3,1}w_{3,1}\right]\right.\\&\quad+c_{12}\left[v_{0,2}+(z-z_0)w_{2,2}+\frac{1}{2}w_{3,2}w_{3,2}\right]\\&\quad\left.-e_{31}E_3-d_{31}H_3\right\}(z-z_0)dz\\&=D_{11}w_{1,1}+D_{12}w_{2,2}+\frac{h}{6}e_{31}\phi_2+\frac{h}{6}d_{31}\psi_2,\end{aligned}$$

$$\begin{aligned}M_{22}(\mathbf{x},\tau)&=\int_0^h\left\{c_{12}\left[u_{0,1}+(z-z_0)w_{1,1}+\frac{1}{2}w_{3,1}w_{3,1}\right]\right.\\&\quad+c_{22}\left[v_{0,2}+(z-z_0)w_{2,2}+\frac{1}{2}w_{3,2}w_{3,2}\right]\end{aligned}$$

$$-e_{32}E_3-d_{32}H_3\}(z-z_0)dz$$
$$=D_{12}w_{1,1}+D_{22}w_{2,2}+\frac{h}{6}e_{32}\phi_2+\frac{h}{6}d_{32}\psi_2,$$
$$M_{12}(\mathbf{x},\tau)=\int_0^h\{c_{66}[u_{0,2}+v_{0,1}+(z-z_0)(w_{1,2}+w_{2,1})+w_{3,1}w_{3,2}]\}(z-z_0)dz$$
$$=\Delta_{11}(w_{1,2}+w_{2,1}), \tag{18}$$

$$T_{11}(\mathbf{x},\tau)=\int_0^h\left\{c_{11}\left[u_{0,1}+(z-z_0)w_{1,1}+\frac{1}{2}w_{3,1}w_{3,1}\right]+c_{12}\left[v_{0,2}+(z-z_0)w_{2,2}+\frac{1}{2}w_{3,2}w_{3,2}\right]-e_{31}E_3-d_{31}H_3\right\}dz$$
$$=c_{11}hu_{0,1}+c_{12}hv_{0,2}+c_{11}h\frac{1}{2}w_{3,1}w_{3,1}+c_{12}h\frac{1}{2}w_{3,2}w_{3,2}+e_{31}\phi_1+d_{31}\psi_1,$$
$$T_{22}(\mathbf{x},\tau)=\int_0^h\left\{c_{12}\left[u_{0,1}+(z-z_0)w_{1,1}+\frac{1}{2}w_{3,1}w_{3,1}\right]+c_{22}\left[v_{0,2}+(z-z_0)w_{2,2}+\frac{1}{2}w_{3,2}w_{3,2}\right]-e_{32}E_3-d_{32}H_3\right\}dz$$
$$=c_{12}hu_{0,1}+c_{22}hv_{0,2}+c_{12}h\frac{1}{2}w_{3,1}w_{3,1}+c_{22}h\frac{1}{2}w_{3,2}w_{3,2}+e_{32}\phi_1+d_{32}\psi_1,$$
$$T_{12}(\mathbf{x},\tau)=\int_0^h\{c_{66}[u_{0,2}+v_{0,1}+(z-z_0)w_{1,1}+w_{3,1}w_{3,2}]\}dz$$
$$=c_{66}h(u_{0,2}+v_{0,1})+c_{66}hw_{3,1}w_{3,2}, \tag{19}$$

$$Q_1(\mathbf{x},\tau)=\kappa\int_0^h c_{55}(w_1+w_{3,1})dz+(T_{11}w_{3,1}+T_{12}w_{3,2})$$
$$=C_1\kappa(w_1+w_{3,1})+(T_{11}w_{3,1}+T_{12}w_{3,2}),$$
$$Q_2(\mathbf{x},\tau)=\kappa\int_0^h c_{44}(w_2+w_{3,2})dz+(T_{21}w_{3,1}+T_{22}w_{3,2})$$
$$=C_2\kappa(w_2+w_{3,2})+(T_{21}w_{3,1}+T_{22}w_{3,2}), \tag{20}$$

where

$$D_{11}=c_{11}\frac{h^3}{12},\quad D_{12}=c_{12}\frac{h^3}{12},$$
$$D_{22}=c_{22}\frac{h^3}{12},\quad \Delta_{11}=c_{66}\frac{h^3}{12},$$
$$C_1=c_{55}h,\quad C_2=c_{44}h. \tag{21}$$

Some terms in the normal and shear forces expressions (19) and (20) are nonlinear since they are given as the products of the deflection gradients and/or normal stresses with deflection gradients. The governing equations have the following form [25,31]:

$$M_{\alpha\beta,\beta}(\mathbf{x},\tau)-Q^l_\alpha(\mathbf{x},\tau)=I_M\ddot{w}_\alpha(\mathbf{x},\tau), \tag{22}$$

$$Q^l_{\alpha,\alpha}(\mathbf{x},\tau)+(T_{\alpha\beta}w_{3,\beta})_{,\alpha}+q(\mathbf{x},\tau)=I_Q\ddot{w}_3(\mathbf{x},\tau), \tag{23}$$

$$T_{\alpha\beta,\beta}(\mathbf{x},\tau)+q_\alpha(\mathbf{x},\tau)=I_Q\ddot{u}_{\alpha0}(\mathbf{x},\tau),\ \mathbf{x}\in\Omega, \tag{24}$$

where the linear part of the shear force is given as

$$Q^l_\alpha=C_\alpha\kappa(w_\alpha+w_{3,\alpha})$$

and

$$I_M=\frac{\rho h^3}{12},\quad I_Q=\rho h,$$

The dots over a quantity indicate differentiations with respect to time τ. A transversal load is denoted by $q(\mathbf{x},\tau)$, and $q_\alpha(\mathbf{x},\tau)$ represents the in-plane loads.

Time-harmonic load is a special case of the general dynamic analysis. Time variation of physical fields is given by the frequency of excitation ω. Then the governing equations for the amplitudes are given by

$$M_{\alpha\beta,\beta}(\mathbf{x},\omega)-Q^l_\alpha(\mathbf{x},\omega)=-I_M\omega^2w_\alpha(\mathbf{x},\omega), \tag{25}$$

$$Q^l_{\alpha,\alpha}(\mathbf{x},\omega)+(T_{\alpha\beta}(\mathbf{x},\omega)w_{3,\beta}(\mathbf{x},\omega))_{,\alpha}+q(\mathbf{x},\omega)=-I_Q\omega^2w_3(\mathbf{x},\omega), \tag{26}$$

$$T_{\alpha\beta,\beta}(\mathbf{x},\omega)+q_\alpha(\mathbf{x},\omega)=-I_Q\omega^2u_{\alpha0}(\mathbf{x},\omega),\quad \mathbf{x}\in\Omega, \tag{27}$$

and the additional set of two governing equations is given by Maxwell equations (10) and (11):

$$e_{31}w_{1,1}(\mathbf{x},\omega)+e_{32}w_{2,2}(\mathbf{x},\omega)-2h_{33}\frac{\phi_2(\mathbf{x},\omega)}{h^2}-2\alpha_{33}\frac{\psi_2(\mathbf{x},\omega)}{h^2}=0,$$
$$d_{31}w_{1,1}(\mathbf{x},\omega)+d_{32}w_{2,2}(\mathbf{x},\omega)-2\alpha_{33}\frac{\phi_2(\mathbf{x},\omega)}{h^2}-2\gamma_{33}\frac{\psi_2(\mathbf{x},\omega)}{h^2}=0. \tag{28}$$

In the rest of the paper we are interesting in static or harmonic load of the MEE plates. The governing Eqs. (25)–(28) represent seven equations for 11 unknowns ($u_0,v_0,w_1,w_2,w_3,\phi_0,\psi_0,\phi_1,\psi_1,\phi_2,\psi_2$). If a problem is symmetric with respect to the neutral plane, the unknowns ϕ_1 and ψ_1 have to be zero and the final set of unknowns is reduced to nine. Now, we need two or four additional equations for a general or symmetric case, respectively. There are two possibilities to prescribe electromagnetic conditions:

(a) The electric displacement D_3 and magnetic induction B_3 are vanishing on both top and bottom surfaces, which gives

$$e_{31}\left[u_{0,1}+w_{1,1}(\mathbf{x},\omega)(h-z_0)+\frac{1}{2}(w_{3,1})^2\right]+e_{32}\left[v_{0,2}+w_{2,2}(\mathbf{x},\omega)(h-z_0)+\frac{1}{2}(w_{3,2})^2\right]-h_{33}\frac{\phi_1(\mathbf{x},\omega)}{h}-2h_{33}\phi_2(\mathbf{x},\omega)\frac{h-z_0}{h^2}-\alpha_{33}\frac{\psi_1(\mathbf{x},\omega)}{h}-2\alpha_{33}\psi_2(\mathbf{x},\omega)\frac{h-z_0}{h^2}=0, \tag{29}$$

$$d_{31}\left[u_{0,1}+w_{1,1}(\mathbf{x},\omega)(h-z_0)\right]+d_{32}\left[v_{0,2}+w_{2,2}(\mathbf{x},\omega)(h-z_0)\right]-\alpha_{33}\frac{\phi_1(\mathbf{x},\omega)}{h}-2\alpha_{33}\phi_2(\mathbf{x},\omega)\frac{h-z_0}{h^2}-\gamma_{33}\frac{\psi_1(\mathbf{x},\omega)}{h}-2\gamma_{33}\psi_2(\mathbf{x},\omega)\frac{h-z_0}{h^2}=0, \tag{30}$$

with ϕ_1 and ψ_1 being vanishing in the symmetric case.
For the non-symmetric case the electric and magnetic potentials can be vanishing on the bottom of the MEE plate. Then, two additional equations are given as

$$\phi_0(\mathbf{x},\omega)-\phi_1(\mathbf{x},\omega)\frac{z_0}{h}+\phi_2(\mathbf{x},\omega)\left(\frac{z_0}{h}\right)^2=0,$$
$$\psi_0(\mathbf{x},\omega)-\psi_1(\mathbf{x},\omega)\frac{z_0}{h}+\psi_2(\mathbf{x},\omega)\left(\frac{z_0}{h}\right)^2=0. \tag{31}$$

In this case the MEE plate is under a mechanical load, and the electromagnetic potentials are induced in the MEE plate. Such plates are used as sensors.

(b) Finite values of potentials, $\tilde{\phi}$ and $\tilde{\psi}$, are prescribed on both surfaces of the plate or for the non-symmetric case on the top surface with vanishing values on the bottom. Now, we need again two or four additional equations. These equations are obtained by collocating potentials on the plate surfaces:

$$\phi(\mathbf{x},h)=\tilde{\phi}=\phi_0(\mathbf{x})+\phi_1(\mathbf{x})\frac{h-z_0}{h}+\phi_2(\mathbf{x})\left(\frac{h-z_0}{h}\right)^2,$$
$$\psi(\mathbf{x},h)=\tilde{\psi}=\psi_0(\mathbf{x})+\psi_1(\mathbf{x})\frac{h-z_0}{h}+\psi_2(\mathbf{x})\left(\frac{h-z_0}{h}\right)^2, \tag{32}$$

with ϕ_1 and ψ_1 being vanishing in the symmetric case, whilst additional equations on the bottom surface are assumed for the non-symmetric case:

$$\phi(\mathbf{x},0)=\tilde{\phi}=\phi_0(\mathbf{x})-\phi_1(\mathbf{x})\frac{z_0}{h}+\phi_2(\mathbf{x})\left(\frac{z_0}{h}\right)^2,$$
$$\psi(\mathbf{x},0)=\tilde{\psi}=\psi_0(\mathbf{x})-\psi_1(\mathbf{x})\frac{z_0}{h}+\psi_2(\mathbf{x})\left(\frac{z_0}{h}\right)^2. \tag{33}$$

It should be noted that only stationary electromagnetic conditions can be prescribed, since stationary Maxwell equations are considered here. The plate under prescribed electromagnetic potentials is deformed and it is used as an actuator. The electric displacement and magnetic induction can be prescribed on both plate surfaces too. Then, in Eqs. (29) and (30) on the right-hand side, prescribed quantities $\tilde{D}_3$ and $\tilde{B}_3$ should be stated.

Instead of writing the global weak-form for the above governing equations, the MLPG methods construct the weak-form over local subdomains such as Ω_s, which is a small region taken for each node inside the global domain [20]. The local subdomains could be of any geometrical shape and size. In the current paper, the local subdomains are taken to be of the circular shape. The local weak-form of the governing Eqs. (25)–(27) for $\mathbf{x}^i\in\Omega_s^i$ can be written as

$$\int_{\Omega_s^i}[M_{\alpha\beta,\beta}(\mathbf{x},\omega)-Q_\alpha^l(\mathbf{x},\omega)+I_M\omega^2 w_\alpha(\mathbf{x},\omega)]w^*_{\alpha\gamma}(\mathbf{x})d\Omega=0, \tag{34}$$

$$\int_{\Omega_s^i}[Q^l_{\alpha,\alpha}(\mathbf{x},\omega)+(T_{\alpha\beta}(\mathbf{x},\omega)w_{3,\beta}(\mathbf{x},\omega))_{,\alpha}+q(\mathbf{x},\omega)+I_Q\omega^2 w_3(\mathbf{x},\omega)]w^*(\mathbf{x})d\Omega=0, \tag{35}$$

$$\int_{\Omega_s^i}[T_{\alpha\beta,\beta}(\mathbf{x},\omega)+q_\alpha(\mathbf{x},\tau)+I_Q\omega^2 u_{\alpha 0}(\mathbf{x},\omega)]w^*_{\alpha\gamma}(\mathbf{x})d\Omega=0, \tag{36}$$

where $w^*_{\alpha\beta}(\mathbf{x})$ and $w^*(\mathbf{x})$ are the weight or test functions.

Applying the Gauss divergence theorem to Eqs. (34)–(36), one obtains

$$\int_{\partial\Omega_s^i}M_\alpha(\mathbf{x},\omega)w^*_{\alpha\gamma}(\mathbf{x})d\Gamma-\int_{\Omega_s^i}M_{\alpha\beta}(\mathbf{x},\omega)w^*_{\alpha\gamma,\beta}(\mathbf{x})d\Omega-\int_{\Omega_s^i}Q^l_\alpha(\mathbf{x},\omega)w^*_{\alpha\gamma}(\mathbf{x})d\Omega$$
$$+\int_{\Omega_s^i}I_M\omega^2 w_\alpha(\mathbf{x},\omega)w^*_{\alpha\gamma}(\mathbf{x})d\Omega=0, \tag{37}$$

$$\int_{\partial\Omega_s^i}Q^l_\alpha(\mathbf{x},\omega)n_\alpha(\mathbf{x})w^*(\mathbf{x})d\Gamma-\int_{\Omega_s^i}Q^l_\alpha(\mathbf{x},\omega)w^*_{,\alpha}(\mathbf{x})d\Omega+\int_{\Omega_s^i}I_Q\omega^2 w_3(\mathbf{x},\omega)w^*(\mathbf{x})d\Omega$$
$$+\int_{\partial\Omega_s^i}T_\beta(\mathbf{x},\omega)w_{3,\beta}(\mathbf{x},\omega)w^*(\mathbf{x})d\Gamma-\int_{\Omega_s^i}T_{\alpha\beta}(\mathbf{x},\omega)w_{3,\beta}(\mathbf{x},\omega)w^*_{,\alpha}(\mathbf{x})d\Omega$$
$$+\int_{\Omega_s^i}q(\mathbf{x},\omega)w^*(\mathbf{x})d\Omega=0, \tag{38}$$

$$\int_{\partial\Omega_s^i}T_\alpha(\mathbf{x},\omega)w^*_{\alpha\gamma}(\mathbf{x})d\Gamma-\int_{\Omega_s^i}T_{\alpha\beta}(\mathbf{x},\omega)w^*_{\alpha\gamma,\beta}(\mathbf{x})d\Omega+\int_{\Omega_s^i}q_\alpha(\mathbf{x},\omega)w^*_{\alpha\gamma}(\mathbf{x})d\Omega$$
$$+\int_{\Omega_s^i}I_Q\omega^2 u_{\alpha 0}(\mathbf{x},\omega)w^*_{\alpha\gamma}(\mathbf{x})d\Omega=0, \tag{39}$$

where $\partial\Omega_s^i$ is the boundary of the local subdomain and

$M_\alpha(\mathbf{x},\omega)=M_{\alpha\beta}(\mathbf{x},\omega)n_\beta(\mathbf{x})$

and

$T_\alpha(\mathbf{x},\omega)=T_{\alpha\beta}(\mathbf{x},\omega)n_\beta(\mathbf{x})$

are the normal bending moment and the traction vector, respectively, and n_α is the unit outward normal vector to the boundary $\partial\Omega_s^i$. The local weak-forms (37)–(39) are the starting point for deriving local integral equations on the basis of appropriate test functions. Unit step functions are chosen for the test functions $w^*_{\alpha\beta}(\mathbf{x})$ and $w^*(\mathbf{x})$ in each subdomain:

$$w^*_{\alpha\gamma}(\mathbf{x})=\begin{cases}\delta_{\alpha\gamma} \text{ at } \mathbf{x}\in(\Omega_s\cup\partial\Omega_s)\\ 0 \text{ at } \mathbf{x}\notin(\Omega_s\cup\partial\Omega_s)\end{cases},\quad w^*(\mathbf{x})=\begin{cases}1 \text{ at } \mathbf{x}\in(\Omega_s\cup\partial\Omega_s)\\ 0 \text{ at } \mathbf{x}\notin(\Omega_s\cup\partial\Omega_s)\end{cases}. \tag{40}$$

Then, the local weak-forms (37)–(39) are transformed into the following local integral equations (LIEs):

$$\int_{\partial\Omega_s^i}M_\alpha(\mathbf{x},\omega)d\Gamma-\int_{\Omega_s^i}Q^l_\alpha(\mathbf{x},\omega)d\Omega+\int_{\Omega_s^i}I_M\omega^2 w_\alpha(\mathbf{x},\omega)d\Omega=0, \tag{41}$$

$$\int_{\partial\Omega_s^i}Q^l_\alpha(\mathbf{x},\omega)n_\alpha(\mathbf{x})d\Gamma+\int_{\Omega_s^i}I_Q\omega^2 w_3(\mathbf{x},\omega)d\Omega+\int_{\partial\Omega_s^i}T_\alpha(\mathbf{x},\omega)w_{3,\alpha}(\mathbf{x},\omega)d\Gamma$$
$$+\int_{\Omega_s^i}q(\mathbf{x},\omega)d\Omega=0, \tag{42}$$

$$\int_{\partial\Omega_s^i}T_\alpha(\mathbf{x},\omega)d\Gamma+\int_{\Omega_s^i}q_\alpha(\mathbf{x},\omega)d\Omega+\int_{\Omega_s^i}I_Q\omega^2 u_{\alpha 0}(\mathbf{x},\omega)d\Omega=0. \tag{43}$$

In the above local integral equations, the trial functions for rotations $w_\alpha(\mathbf{x},\omega)$, transversal displacements $w_3(\mathbf{x},\omega)$ and electromagnetic potential parameters, are chosen as the moving least-squares (MLS) approximations over a number of nodes randomly spreading within the domain of influence.

3. Numerical solution

In general, a meshless method uses a local interpolation to represent the trial function with the values (or the fictitious values) of the unknown variable at some randomly located nodes. The moving least-squares (MLS) approximation [32,33] used in the present analysis may be considered as one of such schemes. According to the MLS method [20], the approximation of the field variable $u\in\{u_0,v_0,w_1,w_2,w_3,\phi_0,\psi_0,\phi_1,\psi_1,\phi_2,\psi_2\}$ can be given as

$$u^h(\mathbf{x})=\sum_{i=1}^{m}p_i(\mathbf{x})a_i(\mathbf{x})=\mathbf{p}^T(\mathbf{x})\mathbf{a}(\mathbf{x}), \tag{44}$$

where $p^T(\mathbf{x})=\{p_1(\mathbf{x}),p_2(\mathbf{x}),\ldots p_m(\mathbf{x})\}$ is a vector of complete basis functions of order m and $a(\mathbf{x})=\{a_1(\mathbf{x}),a_2(\mathbf{x}),\ldots a_m(\mathbf{x})\}$ is a vector of unknown parameters that depends on $\mathbf{x}$. For example, in 2D problems

$\mathbf{p}^T(\mathbf{x})=\{1,x_1,x_2\}$ for $m=3$

and

$\mathbf{p}^T(\mathbf{x})=\{1,x_1,x_2,x_1^2,x_1x_2,x_2^2\}$ for $m=6$

are linear and quadratic basis functions, respectively.

The approximation functions for the generalized mechanical displacements, the electric and magnetic potentials can be written as [20]

$$u^h(\mathbf{x},\omega)=\mathbf{N}^T(\mathbf{x})\cdot\hat{\mathbf{u}}=\sum_{a=1}^{n}N^a(\mathbf{x})\hat{u}^a(\omega), \tag{45}$$

where the nodal values $\hat{u}^a(\omega)$ are fictitious parameters for the approximated field variable and $N^a(\mathbf{x})$ is the shape function associated with node a. The number of nodes n used in the approximation is determined by the weight function $w^a(\mathbf{x})$. A 4th order spline-type weight function is applied in the present work.

The directional derivatives of the approximated field $u(\mathbf{x},\omega)$ are expressed in terms of the same nodal values as

$$u_{,\alpha}(\mathbf{x},\omega)=\sum_{a=1}^{n}\hat{u}^a(\omega)N^a_{,\alpha}(\mathbf{x}). \tag{46}$$

The normal forces expressions (19) include the nonlinear terms proportional to $w_{3,\alpha}w_{3,\beta}$. To linearize the problem the nonlinear terms will be considered in the local integral equations (LIE) iteratively. It means that nonlinear terms computed in the $(k-1)$th iteration are considered in the LIE for kth iteration. According to (46), one obtains the approximation for the bending moments (18) as well as for $M_\alpha(\mathbf{x},\tau)=M_{\alpha\beta}(\mathbf{x},\tau)n_\beta(\mathbf{x})$ or $M(\mathbf{x},\tau)=[M_1(\mathbf{x},\tau),M_2(\mathbf{x},\tau)]^T$ in the kth iteration:

$$\mathbf{M}^{(k)}(\mathbf{x},\omega)=\mathbf{N_1}\sum_{a=1}^{n}\mathbf{B}_1^a(\mathbf{x})\mathbf{w}^{*a(k)}(\omega)+\sum_{a=1}^{n}\mathbf{F}_D^a(\mathbf{x})\hat{\phi}_2^{\;a(k)}(\omega)+\sum_{a=1}^{n}\mathbf{F}_B^a(\mathbf{x})\hat{\psi}_2^{\;a(k)}(\omega), \tag{47}$$

where the vector $w^{*a(k)}(\omega)$ is defined as a column vector $\mathbf{w}^{*a(k)}(\omega)=\left[\hat{w}_1^{a(k)}(\omega),\hat{w}_2^{a(k)}(\omega)\right]^T$, the matrices $N_1(\mathbf{x})$ are related to the normal vector $\mathbf{n(x)}$ on $\partial\Omega_s$ by

$$\mathbf{N}_1(\mathbf{x})=\begin{bmatrix} n_1 & 0 & n_2\\ 0 & n_2 & n_1\end{bmatrix}.$$

Other matrices and vectors in Eq. (47) are represented in terms of the shape functions and their gradients as

$$\mathbf{B}_1^a(\mathbf{x})=\begin{bmatrix} D_{11}N_{,1}^a & D_{12}N_{,2}^a\\ D_{12}N_{,1}^a & D_{22}N_{,2}^a\\ \Delta_{11}N_{,2}^a & \Delta_{11}N_{,1}^a\end{bmatrix},$$

$$\mathbf{F}_D^a(\mathbf{x})=\frac{h}{6}\begin{bmatrix} e_{31}n_1N^a\\ e_{32}n_2N^a\end{bmatrix},\quad \mathbf{F}_B^a(\mathbf{x})=\frac{h}{6}\begin{bmatrix} d_{31}n_1N^a\\ d_{32}n_2N^a\end{bmatrix}. \tag{48}$$

Similarly, one can obtain the approximation for the shear forces

$$\mathbf{Q}^{l(k)}(\mathbf{x},\omega)=\mathbf{C}(\mathbf{x})\kappa\sum_{a=1}^{n}[N^a(\mathbf{x})\mathbf{w}^{*a(k)}(\omega)+\mathbf{L}^a(\mathbf{x})\hat{w}_3^{a(k)}(\omega)], \tag{49}$$

where

$$\mathbf{Q}^{l(k)}(\mathbf{x},\omega)=\left[Q_1^{l(k)}(\mathbf{x},\omega),Q_2^{l(k)}(\mathbf{x},\omega)\right]^T$$

and

$$\mathbf{C}(\mathbf{x})=\begin{bmatrix} C_1(\mathbf{x}) & 0\\ 0 & C_2(\mathbf{x})\end{bmatrix},\quad \mathbf{L}^a(\mathbf{x})=\begin{bmatrix} N_{,1}^a\\ N_{,2}^a\end{bmatrix}.$$

The traction vector $\mathbf{T}^{(k)}(\mathbf{x},\omega)=\left[T_1^{(k)}(\mathbf{x},\omega),T_2^{(k)}(\mathbf{x},\omega)\right]^T$ is approximated by

$$\mathbf{T}^{(k)}(\mathbf{x},\omega)=\mathbf{T}^{l(k)}(\mathbf{x},\omega)+\mathbf{\Sigma}^{(k-1)}(\mathbf{x},\omega)$$

with

$$\mathbf{T}^{l(k)}(\mathbf{x},\omega)=\mathbf{N_1}\sum_{a=1}^{n}\mathbf{P}^a(\mathbf{x})\mathbf{u_0}^{*a(k)}(\omega)+\sum_{a=1}^{n}\mathbf{S}^a(\mathbf{x})\hat{\phi}_1^{\;a(k)}(\omega)+\sum_{a=1}^{n}\mathbf{J}^a(\mathbf{x})\hat{\psi}_1^{\;a(k)}(\omega), \tag{50}$$

where

$$\mathbf{P}^a(\mathbf{x})=h\begin{bmatrix} c_{11}N_{,1}^a & c_{12}N_{,2}^a\\ c_{12}N_{,1}^a & c_{22}N_{,2}^a\\ c_{66}N_{,2}^a & c_{66}N_{,1}^a\end{bmatrix},\quad \mathbf{S}^a(\mathbf{x})=\begin{bmatrix} e_{31}n_1N^a\\ e_{32}n_2N^a\end{bmatrix},\quad \mathbf{J}^a(\mathbf{x})=\begin{bmatrix} d_{31}n_1N^a\\ d_{32}n_2N^a\end{bmatrix},$$

and

$$\mathbf{\Sigma}^{(k-1)}(\mathbf{x},\omega)=h\begin{bmatrix} c_{11}n_1w_{3,1}^{(k-1)}w_{3,1}^{(k-1)}/2+c_{12}n_1w_{3,2}^{(k-1)}w_{3,2}^{(k-1)}/2+c_{66}n_2w_{3,1}^{(k-1)}w_{3,2}^{(k-1)}\\ c_{66}n_1w_{3,1}^{(k-1)}w_{3,2}^{(k-1)}+c_{12}n_2w_{3,1}^{(k-1)}w_{3,1}^{(k-1)}/2+c_{22}n_2w_{3,2}^{(k-1)}w_{3,2}^{(k-1)}\end{bmatrix}.$$

Finally,

$$(T_\alpha(\mathbf{x},\omega)w_{3,\alpha}(\mathbf{x},\omega))^{(k)}=\{\mathbf{T}^{l(k-1)}(\mathbf{x},\omega)+\mathbf{\Sigma}^{(k-1)}(\mathbf{x},\omega)\}^T\times\sum_{a=1}^{n}\mathbf{L}^a(\mathbf{x})\hat{w}_3^{a(k-1)}(\omega).$$

Then, insertion of the MLS-discretized moment, traction and shear force fields (47), (49) and (50) into the local integral Eqs. (41)–(43) yields the discretized local integral equations:

$$\begin{aligned}&\sum_{a=1}^{n}\left[\int_{\partial\tilde{\Omega}_s^i}\mathbf{N}_1(\mathbf{x})\mathbf{B}_1^a(\mathbf{x})d\Gamma-\kappa\int_{\Omega_s^i}\mathbf{C}(\mathbf{x})N^a(\mathbf{x})d\Omega+\mathbf{E}I_M\omega^2\int_{\Omega_s^i}N^a(\mathbf{x})d\Omega\right]\mathbf{w}^{*a(k)}(\omega)\\&-\sum_{a=1}^{n}\hat{w}_3^{a(k)}(\omega)\left(\kappa\int_{\Omega_s^i}\mathbf{C}(\mathbf{x})\mathbf{L}^a(\mathbf{x})d\Omega\right)+\sum_{a=1}^{n}\hat{\phi}_2^{\;a(k)}(\omega)\int_{\partial\tilde{\Omega}_s^i}\mathbf{F}_D^a(\mathbf{x})d\Gamma\\&+\sum_{a=1}^{n}\hat{\psi}_2^{\;a(k)}(\omega)\int_{\partial\tilde{\Omega}_s^i}\mathbf{F}_B^a(\mathbf{x})d\Gamma=-\int_{\tilde{\Gamma}_{sM}^i}\tilde{\mathbf{M}}(\mathbf{x},\omega)d\Gamma,\end{aligned} \tag{51}$$

$$\begin{aligned}&\sum_{a=1}^{n}\left(\kappa\int_{\partial\Omega_s^i}\mathbf{C}_n(\mathbf{x})N^a(\mathbf{x})d\Gamma\right)\mathbf{w}^{*a(k)}(\omega)+\sum_{a=1}^{n}\hat{w}_3^{a(k)}(\omega)\\&\quad\left(\kappa\int_{\partial\Omega_s^i}\mathbf{C}_n(\mathbf{x})\mathbf{L}^a(\mathbf{x})d\Gamma+I_Q\omega^2\int_{\Omega_s^i}N^a(\mathbf{x})d\Omega\right)\\&=-\int_{\Omega_s^i}q(\mathbf{x},\omega)d\Omega-\sum_{a=1}^{n}\hat{w}_3^{a(k-1)}(\omega)\int_{\partial\Omega_s^i}\{\mathbf{T}^{l(k-1)}(\mathbf{x},\omega)\\&\quad+\mathbf{\Sigma}^{(k-1)}(\mathbf{x},\omega)\}^T\mathbf{L}^a(\mathbf{x})d\Gamma,\end{aligned} \tag{52}$$

$$\begin{aligned}&\sum_{a=1}^{n}\left[\int_{\partial\tilde{\Omega}_s^i}\mathbf{N}_1(\mathbf{x})\mathbf{P}^a(\mathbf{x})d\Gamma+\mathbf{E}I_Q\omega^2\int_{\Omega_s^i}N^a(\mathbf{x})d\Omega\right]\mathbf{u}_0^{*a(k)}(\omega)\\&\quad+\sum_{a=1}^{n}\hat{\phi}_1^{\;a(k)}(\omega)\int_{\partial\tilde{\Omega}_s^i}\mathbf{S}^a(\mathbf{x})d\Gamma+\sum_{a=1}^{n}\hat{\psi}_1^{\;a(k)}(\omega)\int_{\partial\tilde{\Omega}_s^i}\mathbf{J}^a(\mathbf{x})d\Gamma\\&=-\int_{\partial\tilde{\Omega}_s^i}\mathbf{\Sigma}^{(k-1)}(\mathbf{x},\omega)d\Gamma-\int_{\tilde{\Gamma}_{sT}^i}\tilde{\mathbf{T}}(\mathbf{x},\omega)d\Gamma-\int_{\Omega_s^i}\mathbf{q}(\mathbf{x},\omega)d\Omega,\end{aligned} \tag{53}$$

in which

$$\mathbf{E}=\begin{bmatrix}1 & 0\\ 0 & 1\end{bmatrix},$$

$\tilde{\mathbf{M}}(\mathbf{x},\tau)$ represents the prescribed bending moments on Γ_{sM}^i, $\tilde{\mathbf{T}}(\mathbf{x},\omega)$ is the prescribed traction vector on Γ_{sT}^i, and

$$\mathbf{C}_n(\mathbf{x})=(n_1,n_2)\begin{pmatrix} C_1 & 0\\ 0 & C_2\end{pmatrix}=(C_1n_1,C_2n_2),$$

Eqs. (51)–(53) are considered on the subdomains adjacent to the interior nodes x^i as well as for the source point x^i located on the global boundary Γ. We point out that

$\partial\tilde{\Omega}_s^i=\partial\Omega_s^i$ and $\tilde{\Gamma}_{sM}^i=\{\emptyset\},\tilde{\Gamma}_{sT}^i=\{\emptyset\};$ if $\mathbf{x}^i\in\Omega$

whilst for the boundary point $x^i\in\Gamma$ we define

$$\partial\tilde{\Omega}_s^i=L_s^i=\partial\Omega_s^i\cap\Omega,\tilde{\Gamma}_{sM}^i=\Gamma_{sM}^i=\partial\Omega_s^i\cap\Gamma_M,\tilde{\Gamma}_{sT}^i=\Gamma_{sT}^i=\partial\Omega_s^i\cap\Gamma_T$$

with $\partial\Omega_s^i=L_s^i\cup\Gamma_{sM}^i\cup\Gamma_{sT}^i$ and Γ_M or Γ_T being the part of the global boundary with prescribed bending moment or in-plane tractions, respectively. If the MEE plate is used as a sensor, the plate is under a mechanical load. Then, the system of the LIE (51)–(53) has to be supplemented by Eqs. (28)–(31). In the kth iteration step the linearized boundary value problem is resolved. Nodal gradients of deflections are computed from Eq. (46), which are used for the evaluation of $\mathbf{\Sigma}^{(k)}$ applied in the next iteration step. The iteration process is stopped if the differences between the deflections in two consecutive steps are less than the prescribed tolerance.

It should be noted here that there are neither Lagrange multipliers nor penalty parameters introduced into the local weak-forms (34)–(36) because the essential boundary conditions on Γ_{sw}^i (part of the global boundary with prescribed rotations or deflection) and Γ_{su}^i (part of the global boundary with prescribed in-plane displacements) can be imposed directly, using the interpolation approximation (45):

$$\sum_{a=1}^{n} N^a(\mathbf{x}^i)\hat{u}^a(\omega) = \tilde{u}(\mathbf{x}^i,\omega) \text{ for } \mathbf{x}^i \in \Gamma^i_{sw} \text{ or } \Gamma^i_{su}, \tag{54}$$

where $\tilde{u}(\mathbf{x}^i,\omega)$ is the prescribed value on the boundary Γ^i_{sw} or Γ^i_{su}. For a clamped plate the rotations and deflection are vanishing on the fixed edge, and Eq. (54) is used at all the boundary nodes in such a case. However, for a simply supported plate only the deflection $\tilde{w}_3(\mathbf{x}^i,\tau)$and bending moments are prescribed, while the rotations are unknowns. Then, the discretized LIE (51) is employed at $\mathbf{x}^i \in \Gamma^i_{sM}$.

If the plate is applied as actuator we use the same Eqs. (51)–(53) and (28) as in the previous case, where the MEE plate is considered as sensor. It should be noted that inertial terms are vanishing in Eqs. (51)–(53), since stationary prescribed potentials are considered here. Eqs. (32) and (33) are applied as additional equations to get a unique formulation of the problem. Collecting the discretized local boundary-domain integral equations together with the discretized boundary conditions for the generalized displacements, bending moment and potentials, one obtains a complete system of algebraic equations.

4. Numerical examples

In the numerical analysis, the coupled MEE plate is assumed to be made of phases $BaTiO_3$ and $CoFe_2O_4$ with 50% volume fraction for each constituent. The following MEE coefficients are considered using the micromechanical theory [34,35]

$$\begin{aligned}
&c_{11} = c_{22} = 21.3 \times 10^{10}\ \mathrm{N\,m^{-2}}, \quad c_{12} = 11.3 \times 10^{10}\ \mathrm{N\,m^{-2}},\\
&c_{33} = 20.7 \times 10^{10}\ \mathrm{N\,m^{-2}}, \quad c_{66} = 5.0 \times 10^{10}\ \mathrm{N\,m^{-2}},\\
&c_{44} = c_{55} = 4.99 \times 10^{10}\ \mathrm{N\,m^{-2}}, \quad e_{31} = e_{32} = -2.71\ \mathrm{C\,m^{-2}},\\
&e_{33} = 8.86\ \mathrm{C\,m^{-2}}, \quad e_{15} = 0.15\ \mathrm{C\,m^{-2}}, \quad d_{31} = d_{32} = 222\ \mathrm{N/A\,m},\\
&d_{33} = 292\ \mathrm{N/A\,m}, \quad d_{15} = 185\ \mathrm{N/A\,m},\\
&h_{11} = 0.24 \times 10^{-9}\ \mathrm{C(V\,m)^{-1}}, \quad h_{33} = 6.37 \times 10^{-9}\ \mathrm{C(V\,m)^{-1}},\\
&\gamma_{11} = 2.01 \times 10^{-4}\ \mathrm{N\,s^2/C^2}, \quad \gamma_{33} = 0.839 \times 10^{-4}\ \mathrm{N\,s^2/C^2},\\
&\alpha_{11} = -5.23 \times 10^{-12}\ \mathrm{N\,s/V\,C}, \quad \alpha_{33} = 2750 \times 10^{-12}\ \mathrm{N\,s/V\,C},\\
&\rho = 5550\ \mathrm{kg}/m^3.
\end{aligned}$$

A square MEE plate with a side-length a=0.254 m is analyzed to verify the proposed computational method. The total thickness of the plate is h=0.012 m. On the top surface a uniform mechanical load is applied. Vanishing electric and magnetic potentials are prescribed on both the bottom and top surfaces of the MEE plate. Lateral sides of the plate have vanishing potentials too. In our numerical calculations, 441 nodes with a regular distribution were used for the approximation of the rotations, deflection, in-plane displacements, electric and magnetic potentials in the neutral plane. The origin of the coordinate system is located at the centre of the plate. Simply supported boundary conditions are considered. The COMSOL computer code is used for the linear FEM analyses with 3364 quadratic elements for one quarter of the plate. FEM results are given only for the linear theory analysis. The variation of the central plate deflection (x_1=x_2=0) with the intensity load is presented in Fig. 2. The intensity load is given by a nondimensional parameter $\tilde{q} = qa^4/c_{11}h^4$. One can observe a good agreement between the FEM and MLPG results for a linear plate bending of the MEE plates. Two different plate thicknesses are considered here. The plate deflection w_3 is normalized by the plate thickness. It can be seen that the plate thickness has only a slight influence on the normalized deflections.

Variations of the electric potential along the x_1-coordinate and along the plate thickness are presented in Figs. 3 and 4 at the nondimensional intensity load $\tilde{q} = 9.42$. At this load intensity one can see clearly that nonlinear effect is apparent. Furthermore the difference of the induced electrical potentials based on the linear and nonlinear theory is more than 20%. Under the linear theory of MEE plates, a good agreement of the FEM and MLPG results is also observed. The maximum electric potential for the simply supported plate reaches at the centre of the plate. The magnetic potential at the plate centre is proportional to the electric potential with ψ/ϕ=0.61 × 10^{-2} and this value corresponds to

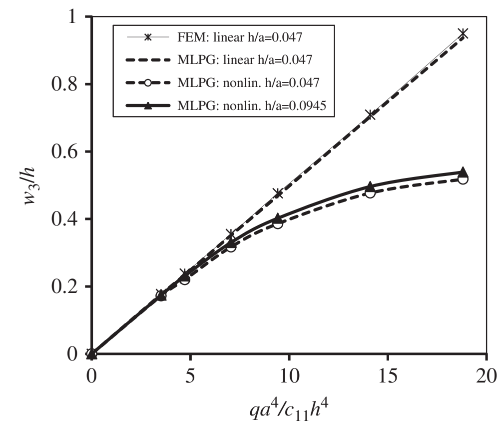

Fig. 2. Variation of the plate deflection at the centre of a simply supported plate with the mechanical load intensity on the top surface.

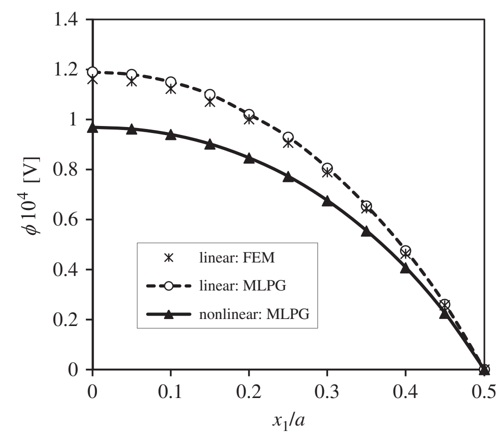

Fig. 3. Variation of the electric potential along the x_1-coordinate for the simply supported plate under the intensity load $\tilde{q} = 9.42$.

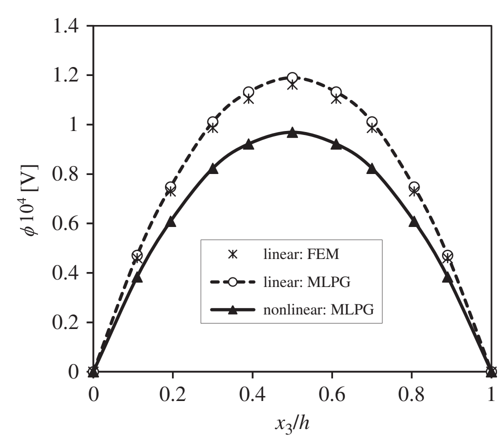

Fig. 4. Variation of the electric potential along the plate thickness for the simply supported plate under the intensity load $\tilde{q} = 9.42$.

the material parameters ratio $d_{31}h_{33}/e_{31}\gamma_{33}$. Therefore, due to this proportional relation, numerical results for magnetic potential are not drawn here.

Next, we analyze the corresponding clamped plate case under the same electromagnetic boundary conditions as for the simply supported plate. The variation of the nondimensional plate deflection at the centre with the nondimensional load intensity is shown in Fig. 5. Compared to the simply supported case (Fig. 2), a significantly large intensity load is required for the clamped plate to get the same deflection value as in the simply supported case.

Variations of the electric potential along the x_1-coordinate as well as along the plate thickness for the clamped plate are presented in Figs. 6 and 7. The induced electrical potential is larger in this case than for the simply supported plate, since the mechanical load intensity is about six times larger for the clamped plate. Both electric potential variations are given at the nondimensional intensity load $\tilde{q}=56.5$. The nonlinearity of the plate deflection has a small influence on the variation of the electric potential. The negative potential in the vicinity of the plate bonding is due to the convex-concave changes of the plate deflection there.

Next, we consider the plate with vanishing electric displacement and magnetic induction, $D_3=0$ and $B_3=0$ on both the top and bottom surfaces. The plate deflection in this case is very similar to that corresponding to prescribed vanishing potentials on both plate surfaces.

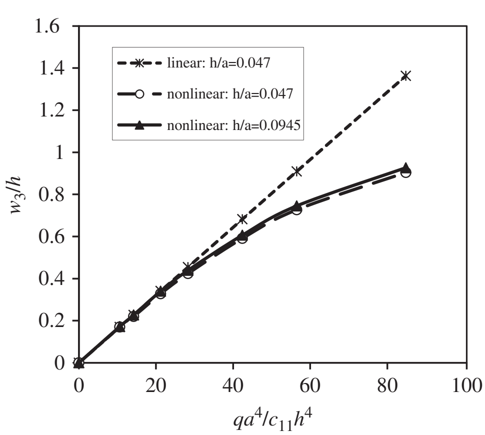

Fig. 5. Variation of the central plate deflection with the load intensity for the clamped plate.

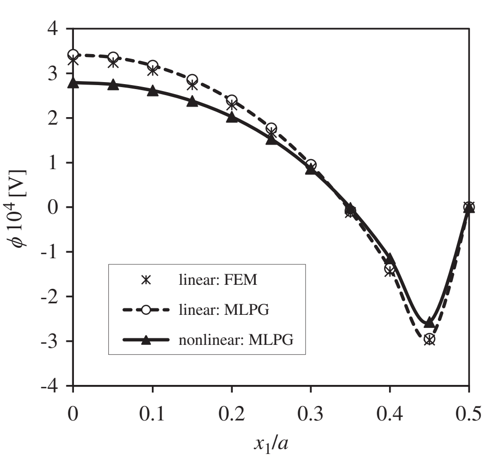

Fig. 6. Variation of the electric potential along the x_1-coordinate for the clamped plate under the intensity load $\tilde{q}=56.5$.

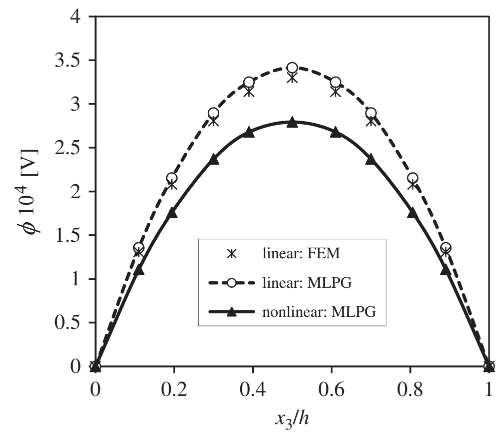

Fig. 7. Variation of the electric potential along the plate thickness for the clamped plate under the intensity load $\tilde{q}=56.5$.

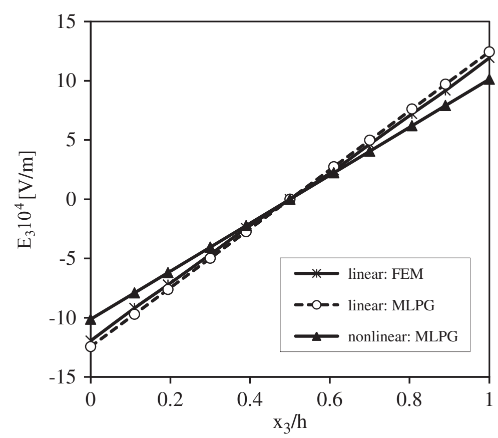

Fig. 8. Variation of the electric intensity along the plate thickness for the clamped plate under intensity load $\tilde{q}=56.5$. Other boundary conditions are $D_3=0$ and $B_3=0$ on both the top and bottom surfaces.

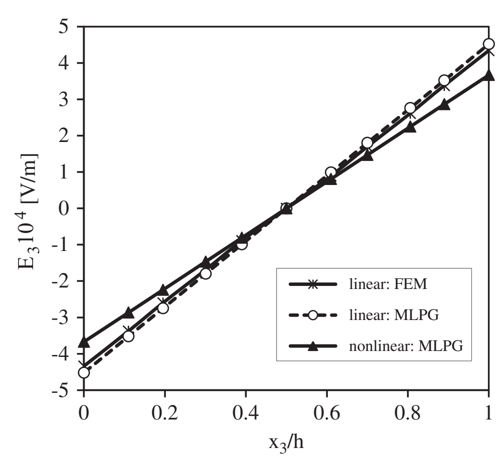

Fig. 9. Variation of the electric intensity along the plate thickness for the simply supported plate at the intensity load $\tilde{q}=9.42$. Other boundary conditions are the same as in Fig. 8.

The variations of the electric intensity vector along the plate thickness are presented in Figs. 8 and 9 for clamped and simply supported plates, respectively. The electric intensity vector E_3 for the case with vanishing electric displacement on the top and bottom plate surfaces is very similar to the electric intensity vector where vanishing potentials are applied on both surfaces.

It means that the difference between both electric potentials is only a constant term corresponding to a potential on both plate surfaces for the case with prescribed electrical displacements. The electromagnetic boundary conditions have a small influence on plate deflection and electric intensity vector.

In the next example we analyze the influence of the harmonic load on the plate deflection. In previous examples, we have seen that the nonlinearity does not change the spatial variation of deflection and potentials; only their maximal values are influenced. Therefore, it is enough to analyze only the linear case. We have selected a small intensity load $\tilde{q}=0.942$ corresponding to a linear case. The nondimensional frequency is defined as, $\omega a/c_s$, where $c_s=(c_{66}/\rho)^{1/2}$ is the velocity of the shear wave. The variation of the deflection with nondimensional frequency for simply supported MEE plate is presented in Fig. 10. Two different plate thicknesses are considered in numerical analyses. One can see that the plate thickness has no influence on the eigenvalue frequency. The comparison of eigenvalue frequencies for simply supported and clamped MEE plates is given in Fig. 11.

In the last numerical example the MEE plate is considered as an actuator with prescribed potentials on both plate surfaces. A nonzero value of the electric potential q_e is prescribed on the top surface, and at the bottom and lateral sides vanishing electric potentials are assumed. The magnetic potentials on all surfaces are vanishing. The variation of the central deflection of the plate ($x_1=x_2=0$) with the electric potential is presented in Fig. 12.

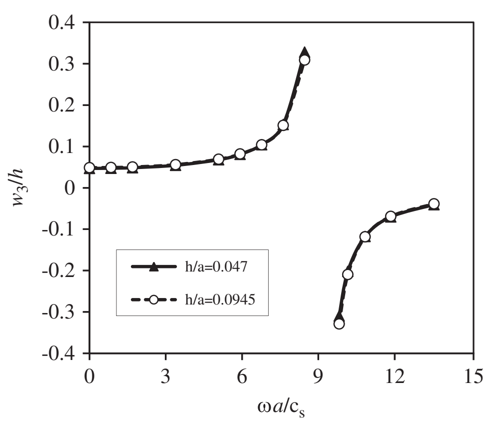

Fig. 10. Variation of the deflection with nondimensional frequency for the simply supported plate under the intensity load $\tilde{q}=0.942$ (linear theory). Other boundary conditions are the same as in Fig. 2.

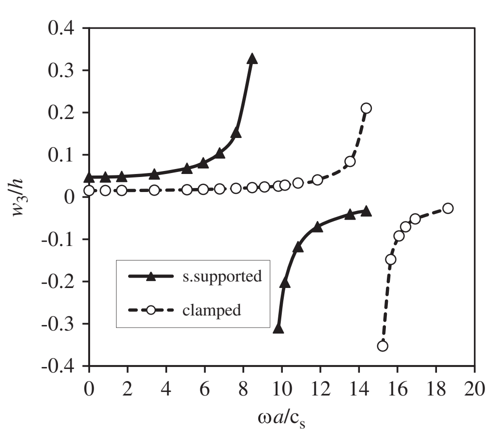

Fig. 11. Resonant frequencies for simply supported and clamped plates at the intensity load $\tilde{q}=0.942$ (linear theory). Other boundary conditions are the same as in Fig. 2.

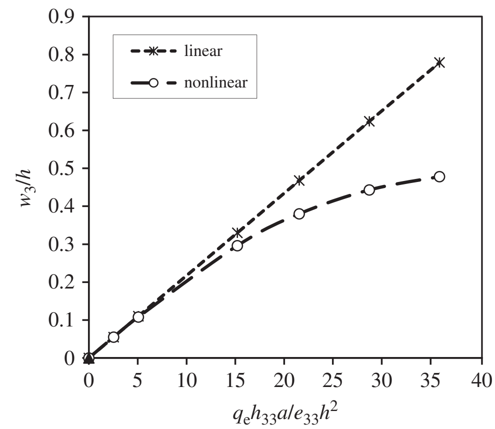

Fig. 12. Variation of the central plate deflection with the prescribed electric potential for the simply supported plate.

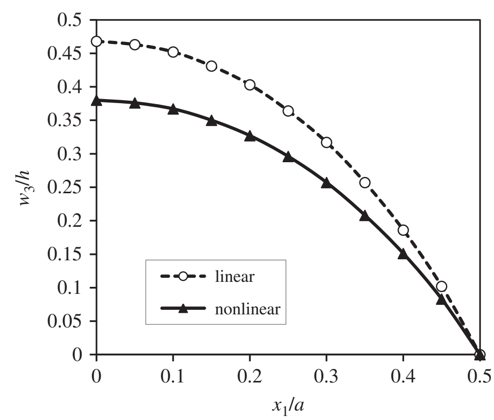

Fig. 13. Variation of the deflection along the x_1-coordinate for the simply supported plate at the intensity of electric potential $\tilde{q}_e=21.55$.

The intensity of the electric potential is given by a nondimensional parameter $\tilde{q}_e=q_e h_{33}a/e_{33}h^2$.

Variation of the deflection along the x_1-coordinate is presented in Fig. 13. Deflections are given at the nondimensional intensity of electrical potential $\tilde{q}_e=21.55$. At this load intensity one can see from Fig. 12 that nonlinear effect is apparent. Therefore, a comparison of linear and nonlinear solutions is interesting. The influence of nonlinearity on the plate deflection at a pure electric load is similar to the case with a pure mechanical load.

5. Conclusions

A meshless local Petrov–Galerkin method is proposed for nonlinear large-deflections of MEE plates under mechanical and magneto-electrical loads. Both the static and time-harmonic boundary value problems are analyzed. von Karman's theory of large deflections is applied for Reissner–Mindlin plates with MEE properties. If a quadratic variation of the electric and magnetic potentials along the plate thickness is assumed, the original 3D thick plate problem is reduced to a 2D problem. Nodal points are randomly distributed over the mean plane of the considered plate. Each node is the centre of a circle surrounding it. The weak form on small subdomains with the Heaviside step function as the test function is applied to derive local integral equations. After performing the spatial MLS approximation, a system of algebraic equations for certain nodal unknowns is obtained.

The proposed method is a truly meshless method, which requires neither domain elements nor background cells in either the interpolation or the integration. It is demonstrated numerically that the quality of the results obtained by the proposed MLPG method is very good. Numerical results are compared with the results obtained by the 3D FEM analyses for linear deflections of MEE plates. The agreement of our numerical results with those obtained by the COMSOL computer code is very good. However, the 3D FEM analysis needs significantly higher number of nodes than in the present formulation.

Numerical results showed that coupling material parameters have a vanishing influence on the plate deflection under a pure mechanical load. Also their influence on the eigen-frequencies is vanishing. Induced electric and magnetic potentials are lower based on the nonlinear large-deformation theory than those in the corresponding linear case; however, their spatial variations in both cases are similar.

Acknowledgements

The authors acknowledge the support by the Slovak Science and Technology Assistance Agency registered under number APVV-0014-10. The authors also gratefully acknowledge the financial assistance of the European Regional Development Fund (ERDF) under the Operational Programme Research and Development/Measure 4.1 Support of networks of excellence in research and development as the pillars of regional development and support to international cooperation in the Bratislava region/ Project No. 26240120020 Building the centre of excellence for research and development of structural composite materials – 2nd stage.

References

[1] Pan E. Exact solution for simply supported and multilayered magneto-electro-elastic plates. ASME J Appl Mech 2001;68:608–18.
[2] Pan E, Heyliger PR. Free vibration of simply supported and multilayered magneto-electro-elastic plates. J Sound Vib 2002;252:429–42.
[3] Wu CP, Chen SJ, Chiu KH. Three-dimensional static behavior of functionally graded magneto-electro-elastic plates using the modified Pagano method. Mech Res Commun 2010;37:54–60.
[4] Liu MF, Chang TP. Closed form expression for the vibration problem of a transversely isotropic magneto-electro-elastic plate. J Appl Mech 2010;77: 24502–10.
[5] Xue CX, Pan E, Zhang SY, Chu HJ. Large deflection of a rectangular magneto electroelastic thin plate. Mech Res Commun 2011;38:518–23.
[6] Timoshenko S, Woinowsky-Krieger S. Theory of plates and shells. New York: McGraw-Hill; 1959.
[7] Sladek J, Sladek V. A meshless method for large deflection of plates. Comput Mech 2003;30:155–63.
[8] Kamiya N, Sawaki Y. An integral equation approach to finite deflection of elastic plates. Int J Non-linear Mech 1982;17:187–94.
[9] Pica A, Wood RD, Hinton E. Finite element analysis of geometrically nonlinear plate behaviour using a Mindlin formulation. Comput Struct 1980;11: 203–15.
[10] Lei XY, Huang MK, Wang X. Geometrically nonlinear analysis of a Reissner type plate by the boundary element method. Comput Struct 1990;37:911–6.
[11] Qin QH. Nonlinear analysis of Reissner plates on an elastic foundation by the BEM. Int J Solids Struct 1993;30:3101–11.
[12] Wen PH, Aliabadi MH, Young A. Post buckling analysis of Reissner plates by the boundary element method. J Strain Anal 2006;41:239–52.
[13] Wen PH, Hon YC. Geometrically nonlinear analysis of Reissener–Mindlin plate by meshless computation. Comput Model Eng Sci 2007;21:177–91.
[14] Pasternak I, Sulym H. Stroh formalism based boundary integral equations for 2D magnetoelectroelasticity. Eng Anal Boundary Elements 2013;37:167–75.
[15] Wen PH, Aliabadi MH. Boundary element formulations for Mindlin plate on an elastic foundation with dynamic load. Eng Anal Boundary Elements 2009;33:1161–70.
[16] Krysl P, Belytschko T. Analysis of thin plates by the element-free Galerkin method. Comput Mech 1996;17:26–35.
[17] Liew KM, Chen XL, Reddy JN. Mesh free radial basis function method for buckling analysis of non-unirormly loaded arbitrarily shaped shear deformable plates. Comput Methods Appl Mech Eng 2004;193:205–24.
[18] Atluri SN, Sladek J, Sladek V, Zhu T. The local boundary integral equation (LBIE) and its meshless implementation for linear elasticity. Comput Mech 2000;25:180–98.
[19] Bishay PL, Sladek J, Sladek V, Atluri SN. Analysis of functionally graded multiferroic composites using hybrid/mixed finite elements and node-wise material properties. Comput Mater Continua 2012;29:213–62.
[20] Atluri SN. The meshless method (MLPG) for domain & BIE discretizations. Encino: Tech Science Press; 2004.
[21] Long SY, Atluri SN. A meshless local Petrov Galerkin method for solving the bending problem of a thin plate. Comput Model Eng Sci 2002;3:11–51.
[22] Sladek J, Sladek V, Wen PH, Aliabadi MH. Meshless Local Petrov–Galerkin (MLPG) Method for shear deformable shells analysis. Comput Model Eng Sci 2006;13:103–18.
[23] Sladek J, Sladek V, Krivacek J, Wen PH, Zhang Ch. Meshless local Petrov–Galerkin (MLPG) method for Reissner–Mindlin plates under dynamic load. Comput Methods Appl Mech Eng 2007;196:2681–91.
[24] Soric J, Li Q, Atluri SN. Meshless local Petrov–Galerkin (MLPG) formulation for analysis of thick plates. Comput Model Eng Sci 2004;6:349–57.
[25] Sladek J, Sladek V, Stanak P, Pan E. The MLPG for bending of electroelastic plates. Comput Model Eng Sci 2010;64:267–98.
[26] Sladek J, Sladek V, Stanak P, Wen PH, Atluri SN. Laminated elastic plates with piezoelectric sensors and actuators. Comput Model Eng Sci 2012;85:543–72.
[27] Azizian ZG, Dawe DJ. Geometrical nonlinear analysis of rectangular Mindlin plates using finite strip method. Comput Struct 1985;21:423–36.
[28] Nan CW. Magnetoelectric effect in composites of piezoelectric and piezomagnetic phases. Phys Rev B 1994;50:6082–8.
[29] Parton VZ, Electromagnetoelasticity BA. Piezoelectrics and electrically conductive solids. New York: Gordon and Breach Science Publishers; 1988.
[30] Batra RC, Liang XQ. The vibration of a rectangular laminated elastic plate with embedded piezoelectric sensors and actuators. Comput Struct 1997;63: 203–16.
[31] Weil NA, Newmark NM. Large deflections of elliptical plates. ASME J Appl Mech 1970;12:1037–51.
[32] Lancaster P, Salkauskas T. Surfaces generated by moving least square methods. Math Comput 1981;37:141–58.
[33] Nayroles B, Touzot G, Villon P. Generalizing the finite element method. Comput Mech 1992;10:307–18.
[34] Kuo HY, Pan E. Effective magnetoelectric effect in multicoated circular fibrous multiferroic composites. J Appl Phys 2011;109:104901.
[35] Kuo HY, Wang YL. Optimization of magnetoelectricity in multiferroic fibrous composites. Mech Mater 2012;50:88–99.